WPJET1-PR(18) 20922

A Czarnecka et al.

Analysis of metallic impurity content by means of VUV and SXR diagnostics in hybrid discharges with hot-spots on the JET-ILW poloidal limiter

Preprint of Paper to be submitted for publication in
Plasma Physics and Controlled Fusion

This work has been carried out within the framework of the EUROfusion Consortium and has received funding from the Euratom research and training programme 2014-2018 under grant agreement No 633053. The views and opinions expressed herein do not necessarily reflect those of the European Commission.

Analysis of metallic impurity content by means of VUV and SXR diagnostics in hybrid discharges with hot-spots on the JET-ILW poloidal limiter

A. Czarnecka[1], N. Krawczyk[1], P. Jacquet[2], E. Lerche[3], V. Bobkov[4], C. Challis[2], D. Frigione[5], J. Graves[6], K. D. Lawson[2], M.J. Mantsinen[7,8], L. Meneses[9], E. Pawelec[10], T. Pütterich[4], M. Sertoli[4, 2], M. Valisa[11], D. Van Eester[3], and JET Contributors[12]

EUROfusion Consortium, JET, Culham Science Centre, Abingdon, OX14 3DB, UK
[1]Institute of Plasma Physics and Laser Microfusion, Hery 23 Str., 01-497 Warsaw, Poland
[2]CCFE, Culham Science Centre, Abingdon, OX14 3DB, UK
[3]Laboratory for Plasma Physics, ERM/KMS, EUROfusion Consortium Member
Renaissancelaan 30, B-1000 Brussels, Belgium
[4]Max-Planck-Institut für Plasmaphysik, Boltzmannstr.2, D-85748, Germany
[5]ENEA, Fusion and Nuclear Safety Dep., C.R. Frascati, Frascati (Roma), Italy
[6]Ecole Polytechnique Fédérale de Lausanne (EPFL), Swiss Plasma Center (SPC), CH-1015 Lausanne, Switzerland
[7]ICREA, Barcelona, Spain,
[8]Barcelona Supercomputing Center, Barcelona, Spain
[9]Associação EURATOM/IST, Instituto de Plasmas e Fusão Nuclear – Laboratório Associado, Instituto Superior Técnico, P-1049-001 Lisboa
[10]Institute of Physics, Opole University, Oleska 48 Str., 45-052 Opole, Poland
[11]Consorzio RFX, Padova, Italy
[12] See the author list of "X. Litaudon et al 2017 Nucl. Fusion 57 102001"

E-mail: agata.czarnecka@ifpilm.pl
Received xxxxxx
Accepted for publication xxxxxx
Published xxxxxx

Abstract

This paper presents a methods for the intrinsic impurity concentration measurements by means of VUV and SXR diagnostics on the JET-ILW tokamak. Measurements of mid-Z impurities content were obtained by means of VUV spectra. To provide absolute concentrations a new relative calibration technique has been proposed. It's based on cross-calibration with a calibrated spectrometer by using the unresolved transition array of W in the relevant wavelength range. The SXR camera was used to deduce W profiles and poloidal asymmetries. To illustrate the importance of high-Z impurity measurements in the development of high performance plasma scenarios, focus is given to hybrid scenario in which strong plasma wall interaction was observed leading to heating of the Be outboard poloidal limiters and the formation of localized hot-spots. This effect was linked to the application of high NBI and ICRH power. In tokamaks with high-Z plasma components, the use of ICRH heating is accompanied by an increased metalic impurity content. Their control in the plasma core is crucial for extending the duration of the high-performance phase of D-T scenarios. Therefore, the impact of the fueling rate, plasma current and separatrix density on hot-spot temperature and the core impurity levels will be discussed. It was found that local D_2 gas injection allows mitigating this effect and run pulses with acceptable temperature values on vessel components. Hot-spot temperature analysis showed a reduced maximum temperature at higher gas rate. A decrease of impurity concentration with D_2 injection rate was observed. Changes in the plasma current have a strong impact on the plasma-wall interaction, both via modifications in the edge density and in the fast-ion losses. Finally it was observed that at constant gas injection rate, both the hot-spots temperature and the core impurity content decrease with the separatrix density.

Keywords: tokamaks, plasma impurity, tungsten, VUV spectroscopy, hot-spots

1. Introduction

Experimental campaigns performed at the tokamak JET in 2015-2016 were devoted to the optimisation of ITER regimes of operation in the presence of the ITER-Like Wall (ILW) and to the optimal preparation of the deuterium-tritium (DT) campaign [1-2]. The development of operational scenarios is underway with the target to provide about 15 MW of maximum fusion power in the forthcoming JET DT experiment, maintaining steady high performance phase for ~5 seconds. This requires i) high power heating, ii) low neutral density (i.e. low gas injection rate and good pumping for weak power degradation of confinement), iii) balance between high plasma current (for high global confinement), and iv) low plasma density (for central beam deposition and high core temperature, $T_i > T_e$). The main challenge to achieve such conditions is high Z impurity accumulation, high divertor heat loads and MHD instabilities. For this purpose, 'baseline' to mean plasmas at high plasma current and, hence, low q_{95} is considered. This plasma scenario takes advantage of the favourable scaling of plasma energy confinement with plasma current to achieve high performance. Also 'hybrid' plasmas at reduced plasma current and, hence, higher q_{95} is developing. In this domain higher normalised pressure (β_N) can be achieved. It was found that higher confinement factor H98(y,2) can be access at higher β_N [3], which helps to compensate for the reduction in plasma current in terms of energy confinement. Operation at higher β_N is challenging in terms of MHD stability. Also, the reduction in plasma current for 'hybrid' plasmas compared with 'baseline' plasmas tends to result in reduced plasma density, which has potential advantages for JET DT because of the improved beam penetration and, hence, central heating. In experiments in 2016, both baseline and and hybrid scenario a new ILW fusion record of 2.9×10^{16} DD neutrons/s was achieved [4]. High-Z impurity control in the core of D-T scenarios with the Ion Cyclotron Resonance Heating (ICRH) was crucial for extending the duration of the high-performance phase [4]. In JET-ILW, core impurity screening can be achieved with high power ICRH heating [5,6]. However, due to RF sheath rectification effects [7] and in some cases fast ion losses (both potentially causing enhanced plasma-wall interaction), increased edge sources are also observed during the application of high power ICRH. For core impurity control, fundamental H minority heating as central as possible with low minority concentration has shown the best results so far in high power H-mode plasmas [5-6,8-9], but dominant N=2 D heating also proved to be effective [11]. He^3 and/or combined H+He^3 minority ICRH heating has shown some promising results in a few cases studied [11] but more experimental investigation is needed to establish these scenarios as a workhorse for impurity control in JET-ILW. The main effects of ICRH that cause reduced impurity peaking are related to temperature peaking, density flattening and fast ion effects [8-10] such as fast ion anisotropy and the collisional processes. Therefore, for plasma operation it is important to characterize the impurity behavior in the confined plasma, as they may lead to radiative cooling and core localized impurity accumulation. In this paper special focus is given to high-power hybrid discharges that were stopped by the real-time vessel protection system due to the formation of hot-spots on the poloidal limiter. Formation of hot-spots on a first wall surface can result in a strong impurity and dust ejection into plasma and discharge termination. The enhanced heat-loads are believed to be related to the joint application of high neutral beams injection (NBI) and ICRH power. Figure 1 is showing the image from a visible camera with the indicated high temperature region on the narrow poloidal limiter NPL3B close to the ICRH antenna B.

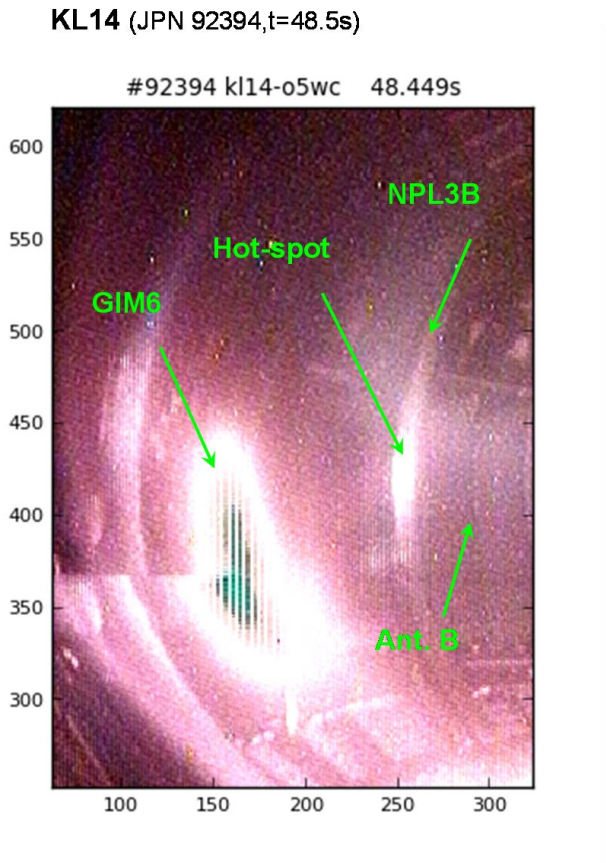

Figure 1. Image form protection camera with the high temperature regions in the poloidal limiter NPL3B.

It was observed that local deuterium (D_2) gas injection from the mid-plane Gas Injection Module (GIM6) allows

reducing hot-spot temperature. Previously obtained experimental results showed that distributed mid-plane gas injection is the best recipe for overall RF coupling improvement at gas levels compatible with high performance scenario development [6, 12, 13]. There are indications that this type of distributed gas injection also has a beneficial impact on RF-induced impurity content but the physics mechanisms behind such observation are still under study [12]. Therefore, both influence of D_2 gas injection on hot-spot temperature and high-, and mid-Z impurity measurements made by means of vacuum-ultra-violet (VUV) and soft X-ray (SXR) diagnostics at JET is presented in this paper.

2. Diagnostics and analysis methods

2.1 VUV/XUV spectroscopy diagnostics

The JET VUV SPRED survey spectrometer [14-15] (known locally as KT2 diagnostic) is routinely used to give impurity data for the operation of the JET machine. The diagnostic has a horizontal line-of-sight (l-o-s) (illustrated in Figure 2 as red line) looking at the vessel mid-plane via an Au coating spherical mirror, allowing it to view the emission from the core and scrape-off layer of the plasma. Signal is detected by a micro-channel plate (MCP) and a phosphor screen from which radiation is coupled by a fiber optic cable to a 2048 pixels Photo Diode Array (PDA). The diagnostic is equipped with a 450 g/mm holographic grating and measures spectra in the 100–1100 Å wavelength range, with a spectral resolution of ~ 5 Å. The highest time resolution is 11 ms, although 50 ms is routinely used. With the carbon plasma facing components (PFC), the long wavelength of VUV spectrum was dominated by low-Z impurities like carbon (C) and oxygen (O), while the short wavelength range by different mid-Z impurities like nickel (Ni), iron (Fe), copper (Cu), chromium (Cr), molybdenum (Mo) making this range particularly valuable from the point of view of diagnosing high temperature plasmas. After installation of the ITER-like wall (ILW) at JET, which consists of a full tungsten (W) divertor and beryllium (Be) main chamber PFCs, the spectrum also contains intense W features (see Figure 3 which shows recorded spectrum in JET Pulse No. (JPN) 92394). The XUV/VUV spectrometer looking from the top of the machine towards the JET divertor, (as illustrated in figure 2) consists of three instruments, two SPRED spectrometers [15] (known locally as KT7/1 and KT7/2) and a Schwob-Fraenkel SOXMOS instrument [16] (known locally as KT7/3). The double SPRED uses 450 g/mm and 2105 g/mm holographic grating, respectively. The higher resolution instrument observes spectra from 140 Å to 443 Å with a spectral resolution of ~1Å. The XUV spectrometer equipped with a 600 g/mm grating, was set to record spectra in the wavelength range 4-7 nm.

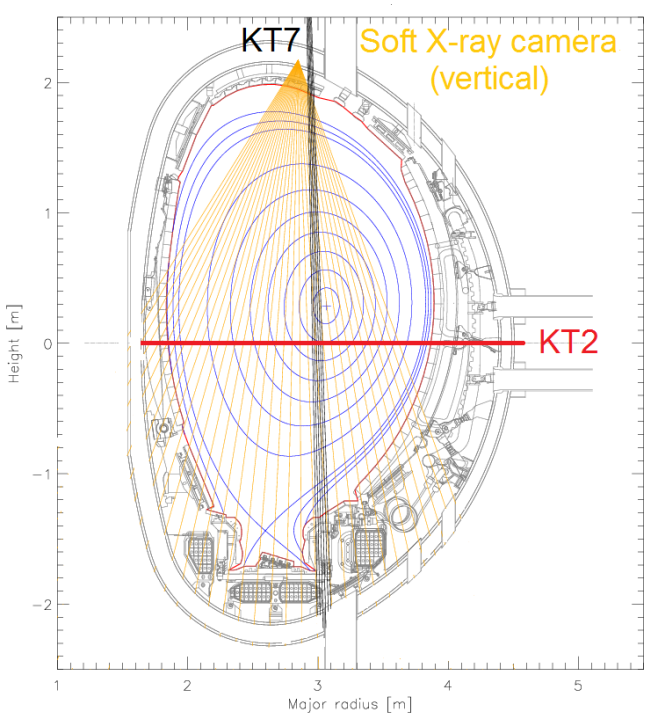

Figure 2. Lines of sight of JET VUV spectrometer (red horizontal line), XUV/VUV spectrometer (black vertical line) and SXR vertical (V) camera (orange lines) at JET tokamak.

2.1.1 New relative calibration method

In order to fully exploit the line intensity measurements, sensitivity calibration of the spectrometer is necessary. In the

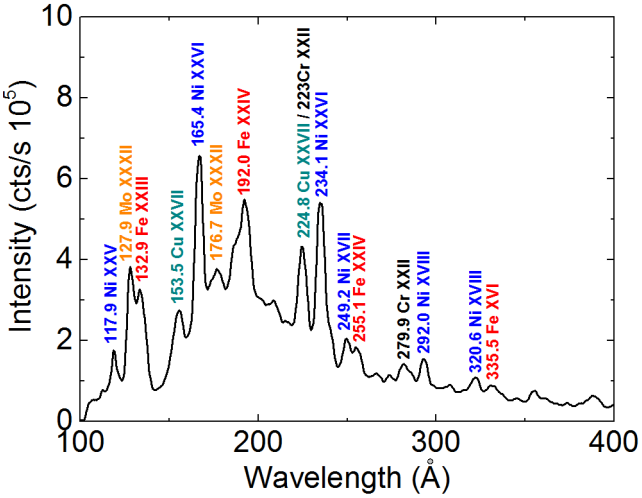

Figure 3. SPRED spectrum in the 100–400 Å wavelength range for JET pulse No 92394 t=8-8.5 s.

case of visible instruments both relative and absolute sensitivity calibrations can be determined using a standard calibration lamp. However, the use of a local calibration source for VUV spectrometers is experimentally very difficult and the removal of vacuum instruments from the machine site

to, for example, a synchrotron source is not possible due to beryllium contamination. As shown by Lawson et al. [17] it is possible to derive absolute sensitivity calibrations using the branching ratio between the C IV 312.4 Å VUV line and the lines at 5801 Å and 5812 Å from a calibrated visible spectrum and use in situ method which involve the use of Na- and Li-like line intensity ratios of different elements to obtain a relative sensitivity curve. The reduction of the C level in the JET-ILW plasmas impacted on the difficulties with the branching ratio technique, because C lines were only occasionally observed, mostly in transient events such as a disruption. Relative intensities are temperature-dependent, which adds the uncertainty to the relative calibrations. This method is also suitable only when lines are well separated, which means that spectrometers with higher spectral resolution are more easily calibrated. Besides, it was found that an independent relative sensitivity calibration of such instrument at JET is unchanged since last calibration [18]. Therefore, to provide absolute mid-Z impurity concentrations a new relative calibration technique is proposed. It is based on cross-calibration with calibrated spectrometer using (simultaneous recordings of) the unresolved transition array (UTA) of W in the relevant wavelength range. Analysis of W ablation experiment shows that around 100 ms after ablation, in sufficiently cold plasma (with maximum temperature not exceeding 2 keV), the same radiating cloud of W is viewed by all the VUV spectrometers with different l-o-s (e.g. horizontal and vertical). This radiation provides a possible tool for cross-calibration of the relative inverse sensitivity of different VUV spectrometers, in the spectral regions where the W radiation is sufficiently strong. This is especially useful for the VUV diagnostic with low spectral resolution and possible line blending (like Ni, Cu lines). In the case of too high core temperature, registered W spectra were too weak to have a proper signal to noise ratio and originated from relatively thin layer of plasma, which may not be symmetric and therefore different for horizontal and vertical l-o-s. As the radiation before and sufficiently after ablation was very similar, the difference of the spectra in studied temporal frames and the frames before ablation were considered as the "pure" ablated W spectrum. Thus the averaged spectra from 100 to 200 ms before and after ablation were subtracted to obtain the pure W spectrum. Curve of inverse sensitivity of KT2 diagnostic was calculated from the ratio of KT2 to KT7/2 spectrum multiplied by inverse sensitivity of KT7/2 diagnostic. Resulting curves obtained for different discharges are presented in figure 4. Tungsten spectra with the new calibration allowed to obtain the same shape of W spectrum from both diagnostics. The calibration results are showing large loss of detector sensitivity in the short-wavelength region in comparison to calibration made for C-wall [17]. It can be also seen, that the shapes of the relative calibration curves are pretty similar for different JET-ILW campaigns, as the pulse numbers cover from 88500 to 92300. Resulting calibration is similar to the

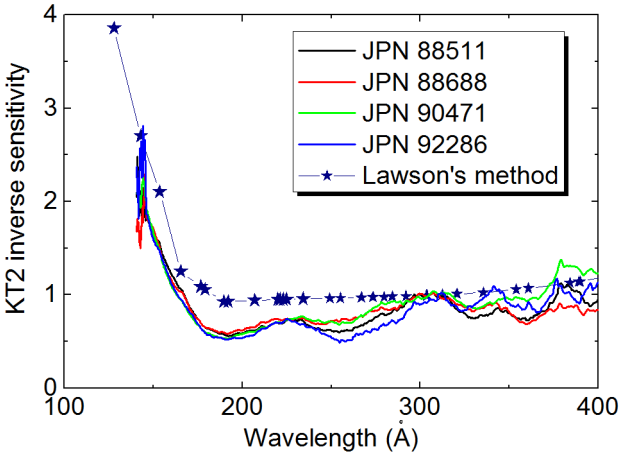

Figure 4. The relative inverse sensitivity calibration at short wavelengths for four pulses with W ablation experiments. Results are compared with calibration curves derived from Na and Li like doublet ratios (S^{-1} at 312.4 Å = 1) using K. Lawson's method presented in [13].

calibration curve obtained using method developed by Lawson et al. The loss of sensitivity at short wavelengths is thought to be due to a deterioration in the grating coating. Less likely explanations are degradation of the CuI coating on the front face of the microchannel plate (MCP) or an absorbing deposited film within the channels themselves. It is noted that throughout the period in which a loss of sensitivity has been observed, the second order spectrum, which is normally absent from SPRED spectra, increased in intensity. This can only be explained by a change in the grating properties, providing further evidence of a change in the grating itself. The 165.4 Å, 192.0 Å and 153.5 Å spectral lines are used to determine respectively Ni, Fe and Cu concentrations in the plasma, using the method described in detail by Czarnecka et al. in Ref. [19]. This technique relies on the absolutely calibrated line intensities measured by the KT2 diagnostics, as well as simulations involving the universal transport code (UTC) [20]. To provide a quantitative measurement of the W-concentration, the XUV spectrometer, which observes a quasicontinuum of the W-ions W^{27+}-W^{35+}, is used. This spectral feature, is emitted at electron temperatures between 0.8-1.8 keV [21]. W concentration is determined, as presented in [22], by taking into account intensity of measured quasicontinuum, proper atomic data for W, the geometry, the electron temperature and density profiles. The VUV and XUV spectrometers provides the intrinsic impurities concentrations that are valid only in a limited radial range, where the ambient T_e allows the ions emission. Furthermore, since measurements are line-integrated, the absolute concentrations inferred from these diagnostics depend on the poloidal distribution of the studied impurities.

2.2 SXR diagnostic

The SXR diagnostic [23] is essential for providing a quantitative estimate of high-Z impurities in the main plasma of JET. Since 2005 SXR system consists of 3 cameras, two with vertical orientation (V, T) and one with horizontal (H). The vertical cameras, due to their favourable viewing geometry are often used for characterization of poloidal asymmetries. Due to technical problem with camera T, the presented results only make use of camera V only. The large number of SXR:V camera l-o-s (presented in figure 2) with maximum acquisition frequency of 0.2 MHz, allows determining the profiles of impurity concentration and the 2D-profiles of SXR-radiation. The l-o-s integrals are performed using their geometry, a magnetic equilibrium reconstruction from EFIT, and taking into account the 250 microns Be filter. Quantitative diagnosis of the W content in this approach is described in detail in Ref. [22]. In order to derive absolute W-concentrations the Bremsstrahlung contribution due to low-Z ions, dominated by D and Be, is subtracted and the excess radiation is attributed to W. This is implemented using the visible Bremsstrahlung Z_{eff} measurements. The recombination radiation contributions are taken into account. For Be they are small. The main disadvantage of the system is the fact that it is not unambiguous what species in the plasma are responsible for the radiation in the soft X-ray range. The heavy impurity proportions cannot be disentangled quantitatively at the moment. This would require a quantitative, spectroscopic evaluation of all contributors with their radial distribution. Thus assuming all SXR contributions beyond Bremsstrahlung is emitted from W is one extreme yielding the highest bolometric implications from the SXR radiator. The physical meaning of the results may be considered preliminary, however, future corrections of the data will not change the main thrust of this paper as most of the conclusions rely on large changes of the soft x-ray emissions, outside of the uncertainties.

2. Results and discussion

All examples discussed here are hybrid discharges with magnetic field B_o=2.76 T, plasma current between I_p=2.2 - 2.4, P_{NBI}=25 MW, and $P_{ICRH} \geq 5$ MW in dipole phasing using simultaneously N=1 H minority ~2% and N=2 D majority. In these conditions, the plasmas are characterized by low collisionality and high q95. Time evolution of the selected parameters for three discharges with constant I_p = 2.2 MA and different D_2 gas injection rate from GIM6, affecting hot spot temperature in the poloidal limiter NPL3B, are presented in figure 5. The hot-spot temperature was measured by infra-red cameras.

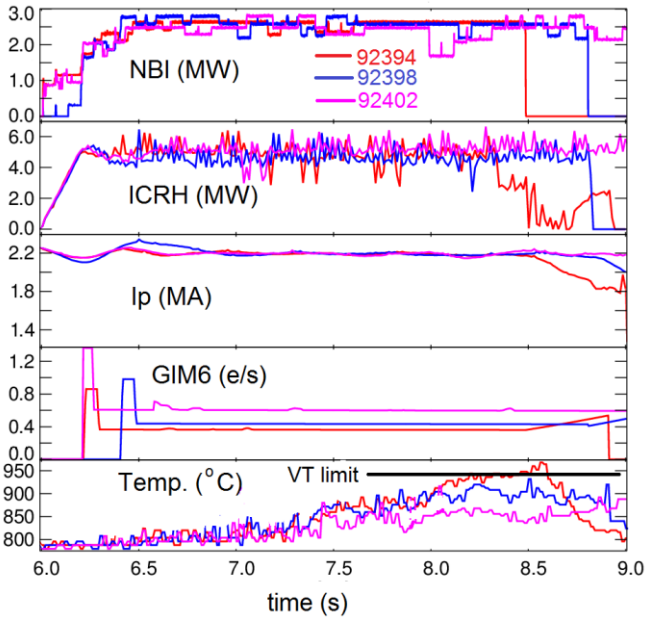

Figure 5. Time evolution of NBI and ICRH heating power, for pulses with the same plasma current Ip=2.2 MA, with different D_2 gas injection from GIM6 and hot spot temperature in the poloidal limiter NPL3B. VT limit is presented as a black horizontal line.

The largest temperature (T_{max}= 940°C) is observed at lowest gas rate in pulse 92394 which was stopped by the real-time wall protection system [24] (VT limit presented in Figure 5). The maximum temperature reached in similar discharges with varying I_p are presented in Figure 6 as function of the D_2 gas injection rate. List of pulses with the time intervals used for the analysis is presented in Table 1. Dedicated investigations showed that hot-spot temperature decreasing with local D_2 gas injection (from GIM6) which helps mitigating hot-spot formation, allowing the pulses to run with acceptable temperature values on protruding vessel components. In addition, at fixed gas injection rate, higher plasma current discharges (characterized by higher separatrix density) are less prone to hot-spot formation. As presented in Figure 7, a decrease of the W (evaluated from the SXR - figure 7a,b and the XUV diagnostics – figure 7c, and mid-Z impurity concentration (in figure 7d-e evaluated from the VUV diagnostic using method described in [19]) with D_2 gas injection rate was equally observed. Ni and Fe impurities come from Inconel or similar Ni based alloys components at the outer main chamber wall. W impurities comes mainly from W divertor and associated divertor baffles but can also be sputtered from plasma facing components located in the main chamber (such as the NBI shine-through protection plates). However, it must be noted that mid-Z and high-Z impurities migrate throughout the vessel and are deposited in the divertor and main chamber limiters. As it can be seen in Figure 7f, the Cu concentrations remains unchanged in this series of discharges. The presence of Cu in JET-ILW high power plasmas in plasmas is associated to the use of the NBI heating.

The error bars presented in Figure 7 are obtained by propagating an uncertainty of the measured line intensity, electron densities and temperatures. The same decreasing trend was observed in the behaviour of the Z_{eff} determined form visible spectroscopy diagnostic (see Figure 8a). Calculations of the contribution of mid-Z impurities to Z_{eff} (ΔZ_{eff}), by the use of data from VUV spectroscopy and the method described in Ref. [19], are presented in Figure 8 b-d). It was found that highest $\Delta Z_{eff} < 0.6$ comes from Ni. Due to high Z of W, its contribution to Z_{eff} is less important in comparison to mid-Z impurities.

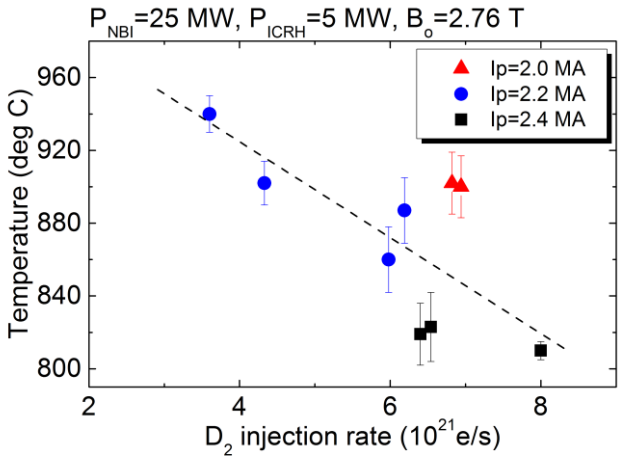

Figure 6. Hot-spot temperature (averaged over time intervals presented in Table 1) on the narrow poloidal limiter NPL3B determined form the protection camera signals as a function of D2 gas injection rate from GIM6.

Table 1 List of JET pulses with time intervals taken for analysis.

JPN	I_p (MA)	time interval (s)
92403	2.0	8.0-8.5
92404	2.0	7.5-8.0
92394	2.2	8.0-8.5
92398	2.2	8.0-8.5
92402	2.2	8.5-9.0
93406	2.2	8.0-8.5
92399	2.4	8.0-8.5
92400	2.4	8.0-8.5
92401	2.4	8.5-9.0

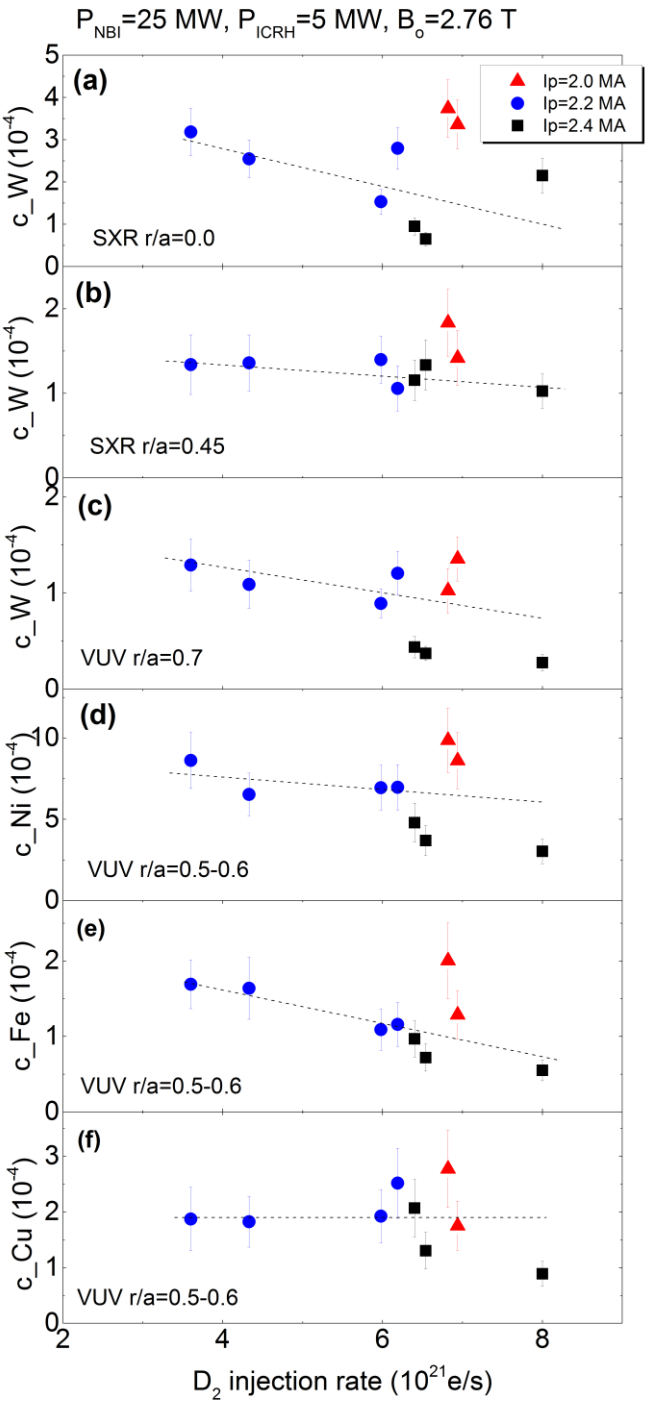

Figure 7. Concentration of a) W at r/a=0.0, b) W at r/a=0.45 derived from the SXR diagnostic, c) W at r/a=0.7 derived from the XUV diagnostic by the use of methods described in [22] and d) Ni at r/a=0.5-0.6, e) Fe at r/a=0.5-0.6, f) Cu at r/a=0.5-0.6 derived from the VUV diagnostic using method described in [19]), as a function of D_2 injection rate for different plasma current I_p (averaged over time intervals presented in Table 1).

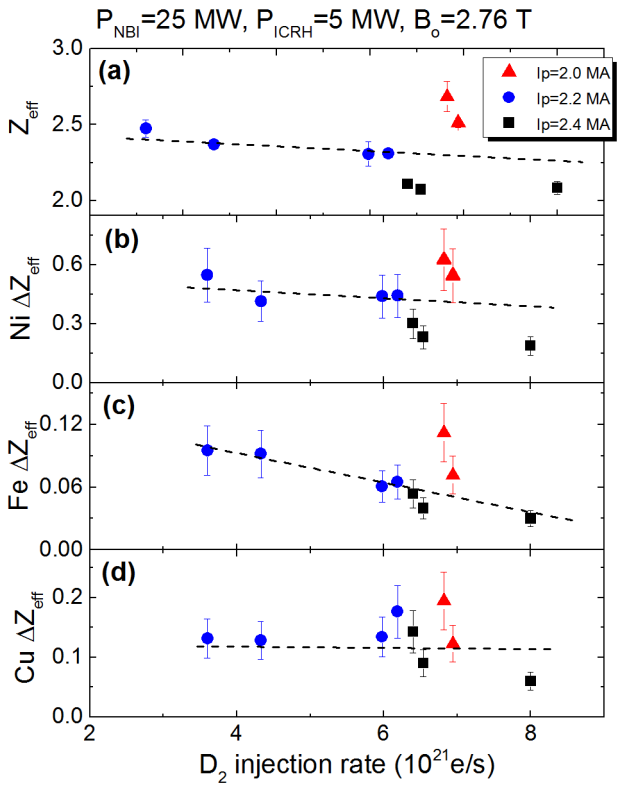

Figure 8. a) Z_{eff} determined form visible spectroscopy diagnostic and contribution of b) Ni, c) Fe, and d) Cu to Z_{eff} determined based on data from VUV spectroscopy diagnostic [19] as a function of D_2 injection rate for different I_p (averaged over time intervals presented in Table 1).

Different trends of the hot spot temperature, impurity concentration and Z_{eff} are observed when plasma current (I_p) was changed. Changes in the I_p have a strong impact on the plasma-wall interaction, via modifications in the edge density. Figure 9 is showing the metallic impurity concentrations in plasmas with different I_p at the same D_2 gas injection rate (~6×10^{21} e/s) as a function of the separatrix density (n_{sep}). It was observed that at constant gas injection rate, both the core metallic impurity content and the hot-spot temperature (not presented here) decrease with the n_{sep}. In Figure 10 the 2D SXR radiation pattern (mainly associated to W in these pulses) is shown for 3 discharges with fixed input power (P_{NBI}=25 MW, P_{ICRH}=5 MW) and different plasma current (and n_{sep}) which time traces are presented in Figure 11. One readily sees that the core W radiation is reduced at higher plasma current and that the poloidal extent of the off-axis radiation region ('mantle') is increased. Poloidal asymmetry within flux surfaces is caused by the centrifugal force on W. Off-axis peaks occur when the radial transport across flux surfaces has a sign inversion near the pedestal top (outward inside the pedestal, inward in the pedestal) [8-10]. This is common in JET shots before the main ion density becomes too peaked and is due to the main ion density gradients which determine

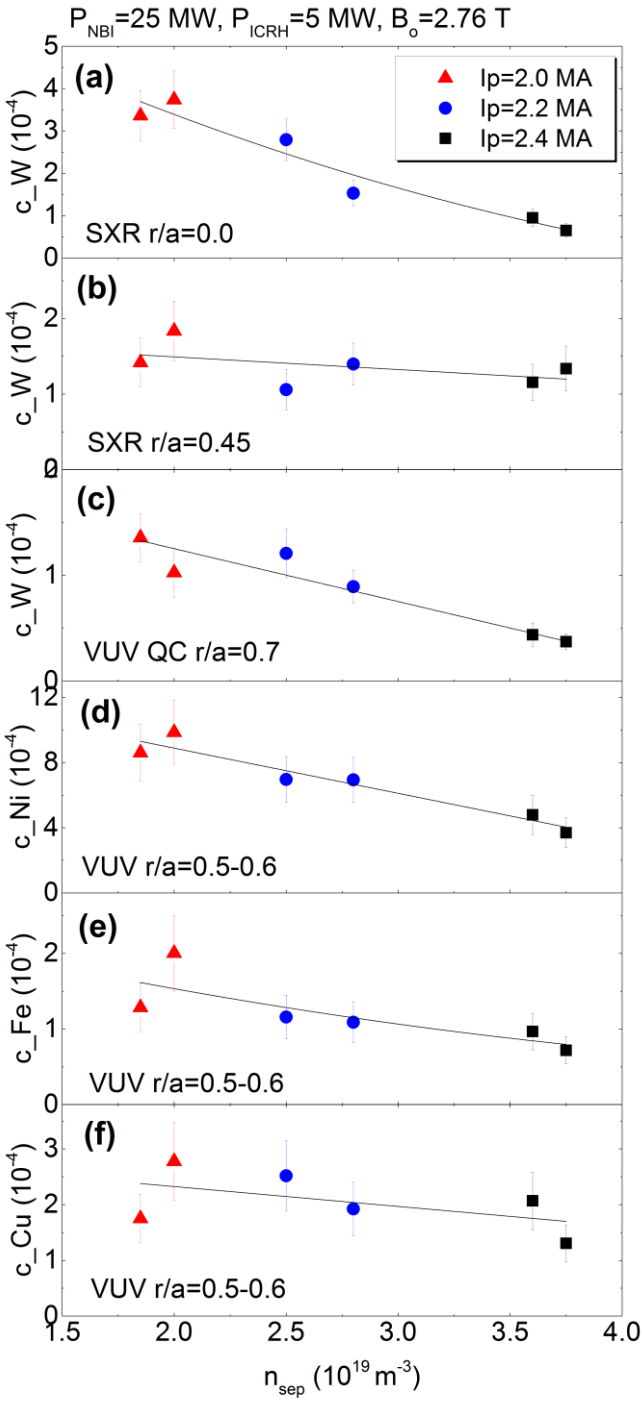

Figure 9. Concentration of a) W at r/a=0.0, b) W at r/a=0.45 derived from the SXR diagnostic, c) W at r/a=0.7 derived from the XUV diagnostic by the use of methods described in [22] and d) Ni at r/a=0.5-0.6, e) Fe at r/a=0.5-0.6, f) Cu at r/a=0.5-0.6 derived from the VUV diagnostic using method described in [19]), as a function of separatrix density for different plasma current I_p (averaged over time intervals presented in Table 1).

the direction of neoclassical convection. When main ion density becomes more peaked, the convection sign can change

and it drives inward W transport and then accumulation on-

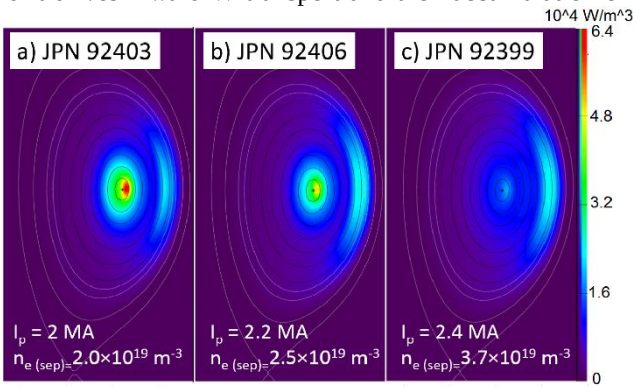

Figure 10. 2D-profiles of SXR-radiation distributed over the JET poloidal cross-section (averaged 0.4 s ~t=8) s for a) JPN 92403 with I_p = 2 MA, n_{sep} =2×10^{19} m^{-3}, b) JPN 92406 with I_p = 2.2 MA, n_{sep} =2.5×10^{19} m^{-3}, and c) JPN 92399 with I_p = 2.4 MA, n_{sep} =3.75×10^{19} m^{-3}.

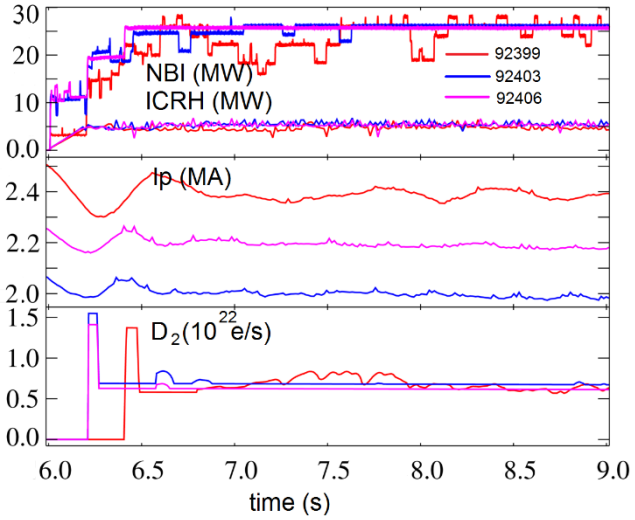

Figure 11. Time evolution of NBI and ICRH heating power, plasma current and D_2 gas injection rate for the selected discharges with different I_p and the same gas injection rate.

axis is observed. In presented cases, the convection reverse direction more than once across the profile. As it can be seen in Figure 12, the rotation velocity evaluated from the observed poloidal in-out asymmetry remains the same for the analysed pulses. Toroidal rotation measurements from charge exchange recombination spectroscopy were not available for the presented pulses. However, consistency checks was performed with the rotation velocity obtained from the high resolution x-ray crystal spectrometer (XCS) (see Figure 12), that observes the spectrum around the resonance line of the helium-like Ni ion. It is possible to see that rotation velocity obtained from the SXR do not match the one from XCS at its radius of measurement. It means that the density calculated from the SXR is not pure W. If the rotation coming out of the SXR is smaller than the measured one from XCS then the contributed impurity has a smaller mass than W. Such observation supports the results showing impact of mid-Z impurity content in the analysed discharges. It should be also noted that poloidal asymmetries, of the W spatial distribution might lead to an underestimation of the W-concentration determined from the VUV diagnostic, however, spectroscopy provides a direct method to determine the W concentration independently of other radiators in the plasma.

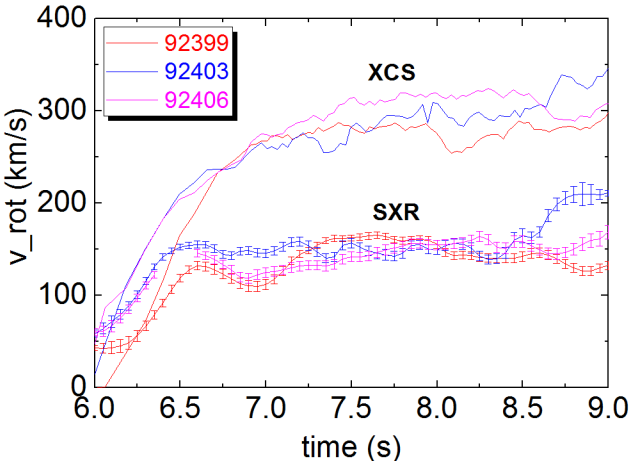

Figure 12. Time evolution of the rotation velocity at r/a=0.45 obtained from the SXR data, and at r/a~0.4 obtained from XCS diagnostic.

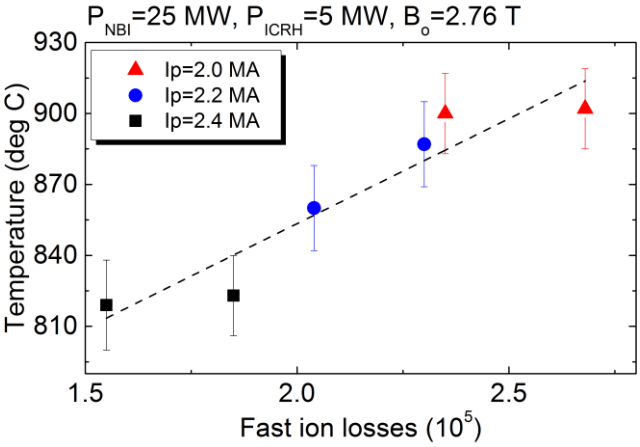

Figure 13. Hot-spot temperature (averaged 0.5 s ~t=8 s) on the narrow poloidal limiter NPL3B determined form the protection camera signals as a function of fast ion losses.

3. Mechanism responsible for the formation of the hot-spots - discussion

The exact mechanism responsible for the formation of the hot-spots is still under investigation. Plasma current and the separatrix density are linked to each other and have a strong impact on the plasma-wall interaction, via changes in the fast-

ion losses and orbit topology. Such effects cannot be disentangled in the experiment. As it can be seen in Figure 13, at constant gas rate hot-spot temperature increase with fast-ion loses, obtained from the fast particle diagnostics measurements, KA3 diagnostic at JET [25]. However, KA3 data do not show a typical ICRH accelerated footprint for D above 200 keV. On the other hand, it has to be noted that only a very small sub-population of D (or D-beam) ions are accelerated to high energies with N=2 ICRH acceleration but they may carry a substantial amount of the RF wave energy. Since there are few particles only but with high energy, to quantify this, full-wave modelling with orbit effects coupled to a 3D Fokker-Planck solver is required which is outside the scope of this paper. Additional studies, presented in [26], shows that there are strong bursts of fusion product ion losses during fishbones instabilities. The detected losses are associated with the highly energetic D-D fusion products (3 MeV protons and 1 MeV tritons).

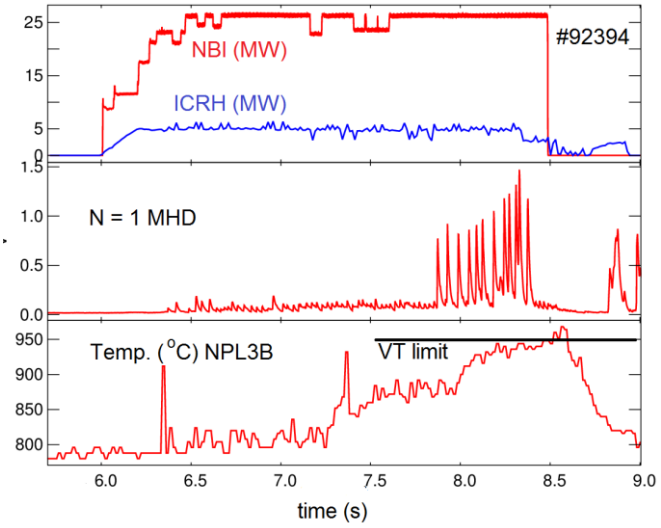

Figure 14. Time evolutions of NBI and ICRH heating power, N = 1 MHD instabilities and hot-spot temperature on the narrow poloidal limiter NPL3B for the JPN 92394 with I_p = 2.2 MA, GIM6 = 3.6e^{21} e/s, n_{sep} = 2.6 e^{19} m^{-3}.

Full orbit analysis presented in [26] indicates that the MeV range ions are likely to hit the wall near the outer mid-plane, that is, close to where the hot-spot on NPL3B is observed and that up to 25 % of the fast fusion product ions can be lost during fishbones. However, the total power associated to fusion products in these pulses is too low (P<=20 kW) to explain the temperature increase observed in the poloidal limiters. Furthermore, although there are pulses for which the hot-spot temperature seems to increase after large fishbones become present (see Figure 14 showing the example of the discharge in which temperature limit was reached causing plasma stop by the protection system there are other examples with considerable hot-spot temperatures which do not respond to the fishbone's onset (see Figure 15). Note that in D-T plasmas, where the fusion power will be significant, the fishbone losses may have a much larger impact on the plasma-wall interaction.

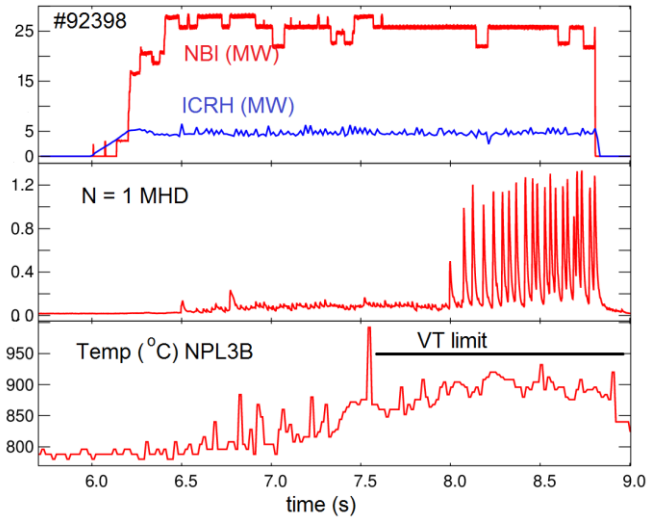

Figure 15. Time evolutions of NBI and ICRH heating power, N = 1 MHD instabilities and hot-spot temperature on the narrow poloidal limiter NPL3B for the JPN 92398 with I_p = 2.2 MA, GIM6 = 4.3e^{21} e/s, n_{sep} = 1.8 e^{19}m^{-3}.

4. Conclusions

In some high power hybrid plasmas, the formation of a hot-spot on the outboard poloidal limiters was observed. On one hand, the heat-loads could be minimized by local gas injection (keeping the total fueling constant) without affecting the core plasma properties, which would suggest that a scrape-of-layer mechanism (e.g. RF sheath effects) is responsible for the enhanced heat-loads observed. The changes in gas affect both hot-spots temperature and impurities concentration. Reduction of hot-spot temperature and metallic impurities content with total D_2 gas injection rate was observed. On the other hand, there is a clear correlation of these quantities with I_p and the separatrix density. For lower I_p (lower n_{sep}), hot-spot temperatures and impurities content are larger than at higher I_p with similar fueling rate. Furthermore, there is also a correlation between the fast particle losses and the heat loads observed in the specific outer wall Be limiters. These observations would suggest that the fast ions impinging in the poloidal limiters come directly from the plasma rather than being accelerated in the scrape-off layer but this is somewhat contradictory with the hot-spot and impurity sensitivity to local gas injection, which does not affect the core profiles and thus is unlikely to affect the fast ion loss mechanisms. One possible explanation is that the fast particle beam that hits a specific region of the limiter is somewhat scattered by the higher SOL density and neutral pressure which causes that the fast ions have a larger probability to collide with an ion or neutrals before hitting the wall. This hypothesis has still to be confirmed. Prompt fusion product losses during large fishbones could also be contributing to the enhanced plasma-wall interaction observed but the power associated to these

reactions is on its own too low to explain the temperature rise observed in the outboard poloidal limiters. In summary, the actual mechanisms causing the heat loads - core losses or scrape-off-layer effects, are not yet understood. Further experimental investigations are planned and the numerical assessment to identify the process involved and help mitigating the formation of hot-spots in future high power hybrid discharges is still ongoing.

Acknowledgements

This work has been carried out within the framework of the EUROfusion Consortium and has received funding from the Euratom research and training programme 2014-2018 under grant agreement No 633053. The views and opinions expressed herein do not necessarily reflect those of the European Commission. This scientific work was partly supported by Polish Ministry of Science and Higher Education within the framework of the scientific financial resources in the year 2018 allocated for the realization of the international co-financed project.

ORCID iDs

A Czarnecka https://orcid.org/0000-0003-4931-728X

References

[1] H. Weisen et al. 2014 AIP Conference Proceedings **1612** 77
[2] L. Horton et al. 2016 Fusion Engineering and Design **109–111** 925
[3] Chalis C et al 2015 Nucl. Fusion **55** 053031
[4] Mantsinen M J et al. 2017 European Physical Journal Web of Conferences **157** 3032
[5] Goniche M et al. (2017) Plasma Physics and Controlled Fusion **59** 055001
[6] Lerche E et al. 2016 Nuclear Fusion **56** 036022
[7] Klepper C C 2013 Journal of Nuclear Materials **438** S594
[8] Angioni C et al., 2014 Nuclear Fusion **54** 083028
[9] Casson F et al. 2015 Plasma Physics and Controlled Fusion **57** 014031
[10] Angioni C et al. 2015 Physics of Plasmas **22** 055902
[11] Van Eester D et al., Proc. 26rd IAEA Fusion Energy, Kyoto, Japan, 17-22 October 2016, IAEA-CN-234, EX/P6-10.
[12] Lerche E et al 2015 Journal of Nuclear Materials **463** 634
[13] Jacquet P et al 2016 Nucl. Fusion **56** 046001
[14] Coffey I H, R. Barnsley R 2004 Rev Sci Instrum **75** 3737
[15] Fonck R J , Ramsey A T, Yelle R V 1982 Appl Optics **21** 2115
[16] Schwob J L et al 1987 Rev. Sci. Instrum. **58** 1601
[17] Lawson K D, Coffey I H, Zacks J, Stamp M F 2009 J. Instrum. **4** P04013
[18] Lawson K D et al. 2011 Plasma Phys. Control. Fusion **53** 015002
[19] Czarnecka A et al. 2011 Plasma Phys. Control. Fusion **53** 035009
[20] Whiteford A D *et al.*, 2004 Proc. 31st EPS Conf., London, UK 28th June - 2nd July, vol. 28G (ECA) P–1.159.
[21] Pütterich T et al 2008 Plasma Phys. and Control. Fusion **50** 085016
[22] Putterich T et al. 2012 Proc. 24rd IAEA Fusion Energy Conf., San Diego, CA 8-13 October 2012 (Vienna: IAEA) vol. IAEA-CN-197, EX–P3.15.
[23] Alper B et al. 1997 Review of Scientific Instruments **68** 778
[24] Valcárcel D.F. et al. 2014 Fusion Engineering and Design **89** 243
[25] Kiptily V G et al. 2009 Nucl. Fusion **49** 065030
[26] Fitzgerald M et al. 2018 "Full-orbit and drift calculations of fusion product losses due to explosive fishbones on JET" submited to Nuclear Fusion
.